

NOTICE

THIS DOCUMENT HAS BEEN REPRODUCED FROM MICROFICHE. ALTHOUGH IT IS RECOGNIZED THAT CERTAIN PORTIONS ARE ILLEGIBLE, IT IS BEING RELEASED IN THE INTEREST OF MAKING AVAILABLE AS MUCH INFORMATION AS POSSIBLE

NASA CR-166735

AYAME/PAM-D
APOGEE KICK MOTOR NOZZLE
FAILURE ANALYSIS

(NASA-CR-166735) AYAME/PAM-D APOGEE KICK
MOTOR NOZZLE FAILURE ANALYSIS (Hadron, Inc.)
29 p HC A03/MF A01 CSCL 21H

N82-10111

Unclas
G3/20 39421

June 22, 1981



Hadron, Incorporated
Systems Management Support Division
1735 Jefferson Davis Highway
Suite 100
Arlington, Virginia 22202

Table of Contents

| | | | |
|--------------|---|----|----|
| 1.0 | Introduction | p. | 1 |
| 2.0 | Ayame I and Ayame II Description | p. | 1 |
| 3.0 | Payload Assist Module (PAM) Description | p. | 2 |
| 4.0 | STAR Series Rocket Motors | p. | 2 |
| | 4.1 Characteristics of the TE-M-364 (STAR 37) | p. | 2 |
| | 4.2 STAR 48 (TE-M-711-3) Motor Description | p. | 3 |
| | 4.3 STAR 37N/STAR 48 Comparison | p. | 8 |
| | 4.4 STAR 48 (DM-2) Failure | p. | 8 |
| 5.0 | SVM Motor Description | p. | 13 |
| 6.0 | Ayame I/Ayame II/KIKU II/STAR 48 (DM-2 Correlation) | p. | 16 |
| 7.0 | Massive Nozzle Failure Postulation | p. | 18 |
| 8.0 | Recapitulation | p. | 21 |
| Appendix I | - Symbology Within Appendices | p. | 23 |
| Appendix II | - Transfer and Geocentric Earth Orbit Values | p. | 24 |
| Appendix III | - Elliptic Equations and Properties | p. | 25 |
| Appendix IV | - Earth Orbital Dynamic Equations and Properties .. | p. | 26 |

1.0

Introduction

In fairly rapid succession, two Japanese communication satellites, Ayame I and II, and the RCA SATCOM III spacecraft failed during the firing sequence of the Apogee Kick Motor (AKM) in such a manner as to suggest a single common casual failure mode. Individual reviews of these three flights have all focused on the failure of the AKM as the single most probable event leading to the nonsuccess of the mission. More recently, the PAM-D upper stage has been incorporated within the configuration of the DELTA launch vehicle; however, its propulsor, the STAR 48 motor, suffered a massive failure during the latter stages of its testing program (DM-2). In view of this pattern, a prudent course of action would be to look at these incidents in unison. As a first step in this direction, the purpose of this independent review is to correlate/compare the circumstances of the Ayame incidents and the failure of the STAR 48 (DM-2) motor, and in the context of a postulated massive nozzle failure of the AKM, determine the impact on spacecraft performance.

2.0

Ayame I and II Description

The launch vehicle for the Ayame I spacecraft was of the three-stage N-1 configuration. The first stage propulsion system was composed of the basic Thor LOX-RP tankage, the Rocketdyne MB-3 motor, and three Castor II strap-ons. The second stage propulsion system essentially consisted of the NASDA/Delta Aerojet N₂O₄-Aerozene 50 rocket motor. The Thiokol STAR 37N solid rocket motor comprised the third stage propulsion system. The AKM for the Ayame I was the Aerojet SVM-2 solid rocket motor. Ayame II was of an identical configuration and served as the back-up for Ayame I. Additional information pertinent to the National Space Development of Japan (NASDA) space program and characteristics of its various space vehicles can be found in the Universal Systems, Inc. (now integrated with Hadron, Inc.) report, "Implications of Ayame Failure for the Delta Project" dated September 7, 1979.

3.0 Payload Assist Module (PAM) Description

The Payload Assist Module (PAM) was developed by McDonnell Douglas on a commercial basis for use either on expendable launch vehicles or for deployment of satellites from the cargo bay of the Space Shuttle. Two versions have been developed. The PAM-D system will be used for spacecraft of the size that will permit either launch by the DELTA or operation from the shuttle whereas the PAM-A will be operated only from the shuttle. When combined with the DELTA 3920, PAM D is capable of lifting a 2750-lb. payload, including the AKM, into a geosynchronous orbit. The propulsion system for the PAM-D is the STAR 48 solid rocket motor developed by Thiokol. The first flight featuring the PAM-D was DELTA 153 and employed the STAR 30B motor as an AKM.

4.0 STAR Series Rocket Motors

The Thiokol STAR series of rocket motors has been utilized in more than 1300 successful flights and has proved to be extremely reliable. With the exception of the STAR 48, the majority of the STAR series are relatively small motors ranging in weight from the approximately 14 lb. STAR 6 (200 successful flights) and 60-lb. STAR 12 (350 successful flights) to the 2470 lb. STAR 37E (51 successful flights). The STAR 37E can be considered a companion motor to the 4660-lb. STAR 48, although the STAR 37E is of somewhat differing design, i.e., front-end ignition, and nozzle material of composite asbestos, glass, and carbon phenolic.

4.1 Characteristics of the TE-M-364 (STAR 37)

The Thiokol TE-M-364 family of rocket motors has as its origin the main retro motor for the Surveyor (Lunar Lander) Program and as such was designated the TE-M-364-1 or STAR 37. The major components of that motor consisted of a spherical steel case of 37 inches diameter, a glass cloth, carbon cloth, and bulk carbon fiber composite impregnated with phenolic resin nozzle, and 1230 lbs. of composite propellant. As the TE-M-364 series expanded, the major changes to the basic motor have been the replacement of the steel case with a titanium case, a variation in the design of the case from the spherical shape

to a more elongated shape depending on the specific mission, an increased propellant weight with some change in its composition, and a modification to the composite nozzle material. The STAR 37N (TE-M-364-14) motor (the NASDA third stage motor for the N-1 configuration) uses the grain configuration (TP-H-3062) and propellant loading (1230 lbs.) of the STAR 37 Surveyor Main Retro, and the motor case (steel) and nozzle components of the STAR 37D (TE-M-364-3). The STAR 37D itself was used as the third stage motor for the DELTA 1913 vehicle. A total of six (6) STAR 37N engines were fabricated of which four (4) were supplied to the Japanese during the 1976-7 time frame. Figures 4.1.1 and 4.1.2 as provided by Thiokol present specification information relative to the STAR 37N.

4.2 STAR 48 (TE-M-711-3) Motor Description

The PAM-D STAR 48 motor comes in two versions. One version, for use during space shuttle missions, contains 4400 pounds of propellant which can be "off loaded" (machined) to a weight of 3833 pounds. The other is for use in Delta-launched missions and has an 8-inch longer nozzle and a propellant weight of 4400 pounds.

The composite propellant used within the STAR 48 is designated TP-H-3340. Its composition and theoretical properties are listed in Figure 4.2.1. It is to be noted that all STAR motor composite propellants, unlike double-based propellants, are very stable and not subject to detonation.

STAR 48 PROPELLANT COMPOSITION AND THEORETICAL PROPERTIES

| | |
|------------------------------------|--------|
| COMPOSITION | HTPB |
| SOLIDS, % | 89 |
| AI, % | 18 |
| AP, % | 71 |
| HMX, % | - |
| THEORETICAL PROPERTIES (1000 PSIA) | |
| ISP ($\xi = 50$), SEC | 290.6 |
| C*, FT/SEC | 5223 |
| T _f , °F | 6113 |
| ρ , LB/IN. ³ | 0.0655 |

Figure 4.2.1



The STAR 37N motor uses the grain configuration and propellant loading of the STAR 37 Surveyor Main Retro and the motor case and nozzle components of the STAR 37D Improved Delta Third Stage.

MOTOR PERFORMANCE

| | |
|---|-----------|
| Burn Time/Action Time (t_b/t_a), sec | 37.5/39.0 |
| Ignition Delay Time (t_d), sec | 0.160 |
| Burn Time Avg. Cham. Press. (P_b), psia | 560 |
| Action Time Avg. Cham. Press. (P_a), psia | 540 |
| Maximum Chamber Pressure (P_{max}), psia | 620 |
| Total Impulse (I_T), lbf-sec | 357,600 |
| Propellant Specific Impulse (I_{sp}), lbf-sec/lbm | 290.2 |
| Effective Specific Impulse, lbf-sec/lbm | 287.8 |
| Burn Time Average Thrust (\bar{F}_b), lbf | 8,900 |
| Maximum Thrust (F_{max}), lbf | 9,600 |

WEIGHTS, lbm

| | |
|---|-------|
| Total Loaded | 1,372 |
| Propellant | 1,232 |
| Case Assembly | 69.9 |
| Nozzle Assembly | 47.1 |
| Igniter Assembly (with mechanical S&A) | 5.2 |
| Internal Insulation | 15.0 |
| Liner | 1.0 |
| Miscellaneous | 1.8 |
| Total Inert (igniter propellant not included) | 140.0 |
| Burnout | 129.5 |
| Propellant Mass Fraction | 0.90 |

TEMPERATURE LIMITS

| | |
|-----------|---------------|
| Operation | 30°F to 90°F |
| Storage | 40°F to 100°F |

•75°F, Vacuum, 110 rpm

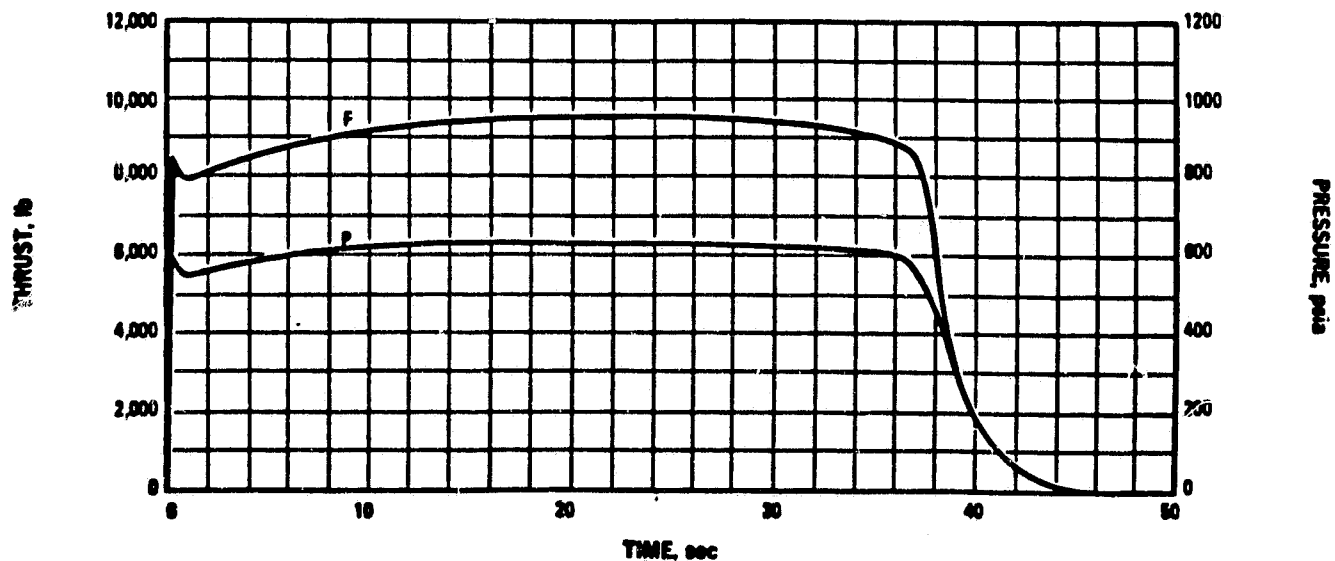
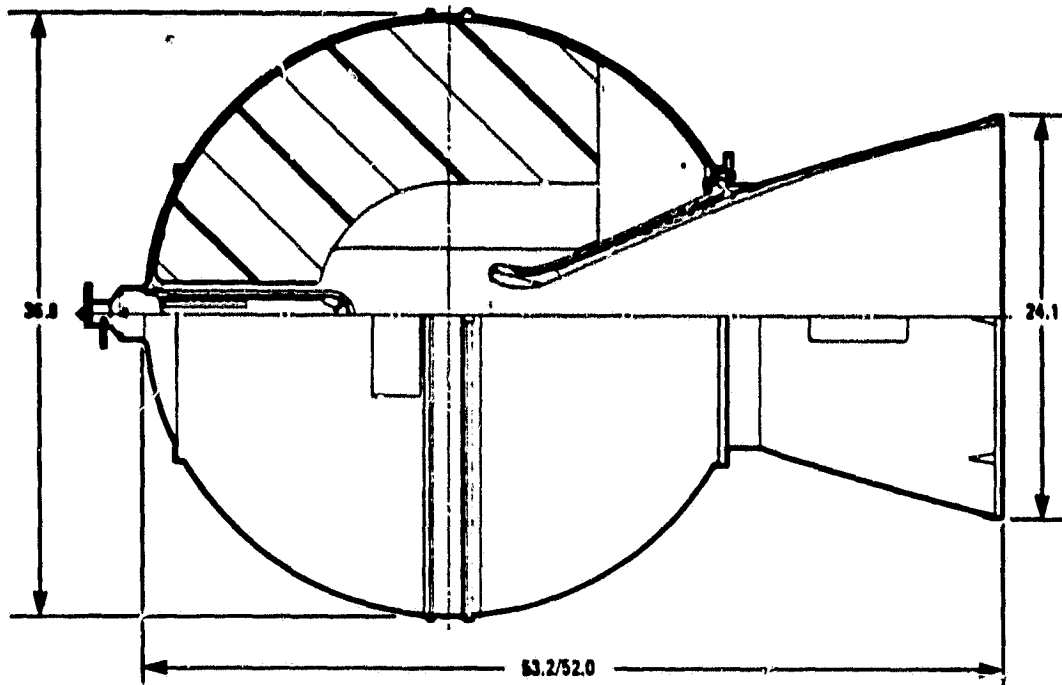


Figure 4.1.1

ORIGINAL PAGE IS
OF POOR QUALITY



CASE

| | |
|--|-------------------|
| Material | Ladish DGAC Steel |
| Minimum Ultimate Strength, psi | 220,000 |
| Minimum Yield Strength, psi | 200,000 |
| Hydrostatic Test Pressure, psi | 707 |
| Minimum Burst Pressure, psi | 885 |
| Hydrostatic Test Pressure/Maximum Pressure | 1.05 |
| Burst Pressure/Maximum Pressure | 1.25 |
| Nominal Thickness, in. | 0.039 |

NOZZLE

| | |
|--|---|
| Body Material | Composite Glass Cloth & Carbon Cloth Impregnated with Phenolic Resin |
| Throat Insert Material | Graph-I-Tite G-90 |
| Initial Throat Diameter, in. | 3.29 |
| Exit Diameter, in. | 24.1 |
| Expansion Ratio, Initial/Final | 53.2/52.0 |
| Expansion Cone Half Angles, Exit/EN, deg | 14.2/16.1 |
| Type | Fixed |
| Number of Nozzles | 1 |

LINER

| | |
|-------------------------------|----------|
| Type | TL-H-304 |
| Density, lbm/in. ³ | 0.046 |

IGNITER

| | |
|---------------------------|----------|
| Thiokol Model Designation | TE-P-358 |
| Type | Pyrogen |

PROPELLANT

| | |
|--|-----------|
| Propellant Designation and Formulation | TP-H-3062 |
| CTPB Binder - 14% | |
| Al - 16% | |
| AP - 70% | |

PROPELLANT CONFIGURATION

| | |
|--|--------------|
| Type | 7-Point Star |
| Web, in. | 10.18 |
| Web Fraction, % | 56 |
| Sliver Fraction, % | 2.6 |
| Propellant Volume, in. ³ | 19,700 |
| Volumetric Loading Density, % | 76.0 |
| Web Average Burning Surface Area, in. ² | 1,885 |
| Initial Surface to Throat Area Ratio (K ₀) | 213 |

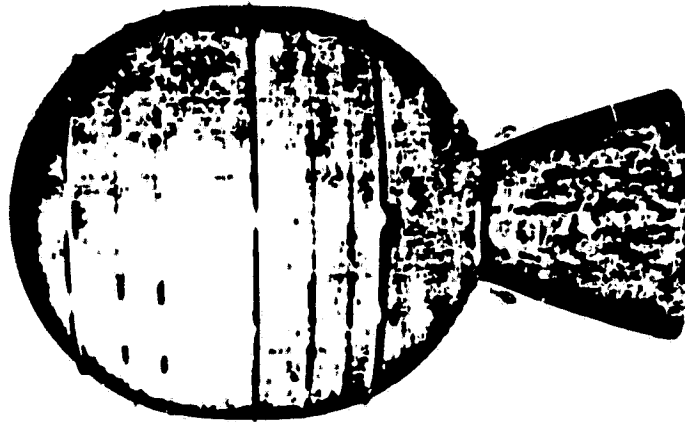
PROPELLANT CHARACTERISTICS

| | |
|--|--------------|
| Burn Rate @ 1000 psia (r _b), in./sec | 0.301 |
| Burn Rate Exponent (n) | 0.31 |
| Density, lbm/in. ³ | 0.0628 |
| Temperature Coefficient of Pressure (α_k), %/°F | 0.10 |
| Characteristic Exhaust Velocity (C*), ft/sec | 5,025 |
| Adiabatic Flame Temperature (T _f), °F | 5,642 |
| Effective Ratio of Specific Heats (Chamber) (Nozzle Exit) | 1.15 1.21 |

CURRENT STATUS

Production

9/78



The STAR 48 motor is being developed for the McDonnell Douglas Payload Assist Module (PAM). The basic version (TE-M-711-3), planned for STS missions, contains 4400 pounds of propellant and has an overall length of 73 inches. Offload capability to 3833 pounds of propellant (TE-M-711-4) will also be qualified. Versions with an 8-inch-longer nozzle, one fully loaded (TE-M-711-8), and one offloaded to 3844 pounds of propellant (TE-M-711-9), will be qualified for use in Delta-launched missions.

MOTOR PERFORMANCE*

| | |
|--|-----------|
| Burn Time/Action Time (t_b/t_a), sec | 84.0/85.3 |
| Ignition Delay Time (t_d), sec | 0.05 |
| Burn Time Avg Chamber Pressure (P_b), psia | 588 |
| Action Time Avg Chamber Pressure (P_a), psia | 585 |
| Maximum Chamber Pressure (P_{max}), psia | 634 |
| Total Impulse (I_T), lbf-sec | 1,280,000 |
| Burn Time Impulse (I_b), lbf-sec | 1,260,000 |
| Propellant Specific Impulse, lbf-sec/lbm | 290.7 |
| Effective Specific Impulse, lbf-sec/lbm | 289.3 |
| Burn Time Average Thrust (F_b), lbf | 15,000 |
| Action Time Average Thrust (F_a), lbf | 14,980 |
| Maximum Thrust (F_{max}), lbf | 17,200 |

Note: TE-M-711-8 motor with 8-inch-longer nozzle delivers an effective I_{sp} of 294.1 lbf-sec/lbm

70°F, vacuum, 100 rpm

WEIGHTS, lbm

| | |
|--|-------|
| Total Loaded | 4660 |
| Propellant | 4402 |
| Case Assembly | 129 |
| Nozzle Assembly | 39 |
| Internal Insulation | 60 |
| Liner | 3 |
| S&A/ETA | 5 |
| Miscellaneous | 3 |
| Total Inert (excluding igniter propellant) | 258 |
| Burnout | 235 |
| Propellant Mass Fraction | 0.945 |

TEMPERATURE LIMITS

| | |
|-----------|-------------|
| Operation | 30 to 110°F |
| Storage | 60 to 100°F |

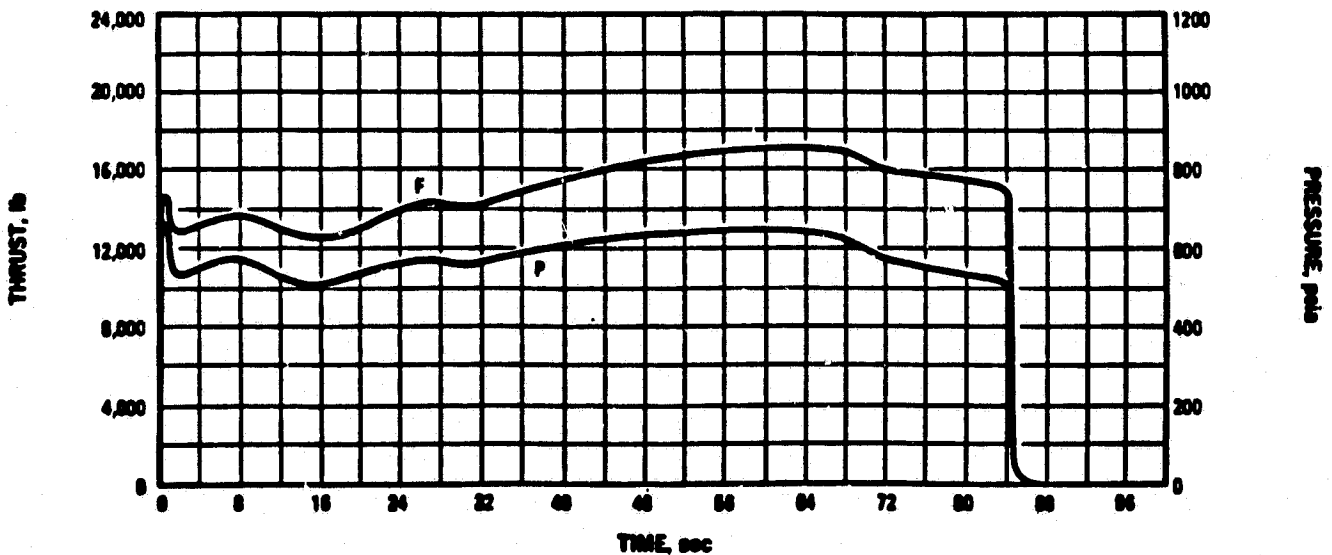
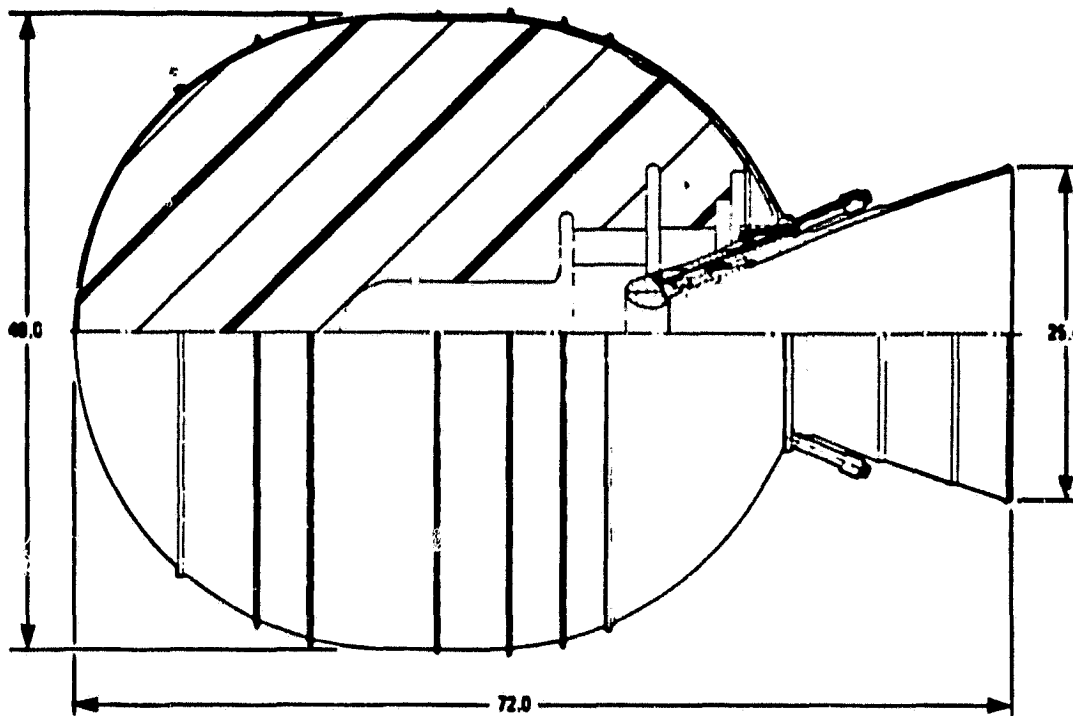


Figure 4.2.2

ORIGINAL PAGE IS
OF POOR QUALITY



CASE

| | |
|--|-----------------|
| Material | 6Al-4V Titanium |
| Minimum Ultimate Strength, psi | 165,000 |
| Minimum Yield Strength, psi | 155,000 |
| Hydrostatic Test Pressure, psi | 732 |
| Minimum Burst Pressure, psi | 860 |
| Hydrostatic Test Pressure/Maximum Pressure | 1.05 |
| Burst Pressure/Maximum Pressure | 1.25 |
| Nominal Thickness, in. | 0.069 |

NOZZLE

| | |
|--|-------------------|
| Exit Cone Material | 2-D Carbon/Carbon |
| Throat Inert Material | Graph-I-Tite G-90 |
| Initial Throat Diameter, in. | 3.88 |
| Exit Diameter, in. | 26.06 |
| Expansion Ratio, Initial/Average | 39.6/35.0 |
| Expansion Cone Half Angles, Exit/Exit, deg | 16.5/18.1 |
| Type | Fixed Contoured |
| Number of Nozzles | 1 |

LINER

| | |
|-------------------------------|----------|
| Type | TL-H-318 |
| Density, lbm/in. ³ | 0.038 |

IGNITER

| | |
|---------------------------------|--|
| Thiokol Model Designation | Model 2130 S&A |
| Type | S&A/ETA/TBI/Initiator/Toroidal Pyrogen |
| Minimum Firing Current, amperes | 5.0 |
| Circuit Resistance, ohms | 1.1 |
| No. of Detonators and TBI's | 2 |

PROPELLANT

| | |
|--|-----------|
| Propellant Designation and Formulation | TP-H-3340 |
| Al - 18% | |
| AP - 71% | |
| HTPB Bladder - 11% | |

PROPELLANT CONFIGURATION

| | |
|--|---------------------------------------|
| Type | Internal-Burning, Radial-Slotted Star |
| Web, in. | 20.47 |
| Web Fraction, % | 84 |
| Sliver Fraction, % | 0 |
| Propellant Volume, in. ³ | 67,590 |
| Volumetric Loading Density, % | 82.6 |
| Web Average Burning Surface Area, in. ² | 3300 |
| Initial Surface to Throat Area Ratio (K ₀) | 217 |

PROPELLANT CHARACTERISTICS

| | |
|---|--------|
| Burn Rate @ 1000 psia (r _B), in. /sec | 0.282 |
| Burn Rate Exponent (n) | 0.30 |
| Density, lbm/in. ³ | 0.0651 |
| Temperature Coefficient of Pressure (T _k), %/°F | 0.10 |
| Characteristic Exhaust Velocity (C*), ft/sec | 5120 |
| Adiabatic Flame Temperature (T _f), °F | 6113 |
| Effective Ratio of Specific Heats (Chamber) | 1.13 |
| (Nozzle Exit) | 1.18 |

CURRENT STATUS

Development

7/79

Figure 4.2.3

The specifications for the STAR 48 motor are itemized in Figures 4.2.2 and 4.2.3. Of special note pertinent to this study is the 2-D carbon/carbon exit cone material.

4.3 STAR 37N/STAR 48 Comparison

Significant differences exist between these two motors. The STAR 37N is a hybrid assembly of proven components but represents older technology; whereas, the STAR 48 is a more recent development and incorporates the latest state-of-art with respect to materials and design. Figure 4.3.1 reflects a comparison of the more prominent characteristics of each.

| <u>STAR 37N</u> | | <u>STAR 48</u> |
|---|-------------------------------|---------------------|
| 37.5 sec | BURN TIME | 84.0 sec |
| 357,500 lbf-sec | TOTAL IMPULSE | 1,260,000 lbf-sec |
| 9,600 lbf | MAXIMUM THRUST | 17,200 lbf |
| 1,372 lb. | TOTAL WEIGHT | 4,660 lb. |
| 1,232 lb. | PROPELLANT WEIGHT | 4,402 lb. |
| TP-H-3062 | PROPELLANT DESIGNATION | TP-H-3340 |
| 7-point Star | PROPELLANT TYPE CONFIGURATION | Radial Slotted Star |
| Ladish D6AC Steel | CASE MATERIAL | 6Al-4V Titanium |
| Composite Glass Cloth and Carbon Cloth Impreg. Phenolic Resin | NOZZLE EXIT CONE | 2D Carbon/Carbon |
| Graph-I-Tite E-90 | NOZZLE THROAT INSERT MATERIAL | 3D Carbon/Carbon |

Figure 4.3.1

Because of their dissimilarities, little correlation exists between these two motors. As previously stated, the STAR 37N was developed solely for the Japanese N-1 configuration. Only six were constructed and all have been expended. No difficulties were encountered by the Japanese regarding 37N operation. Since the Japanese have progressed to the N-2 configuration it is unlikely that 37N production will be reinitiated. As a result, no further attempt will be made to establish a correlation between the STAR 37N and the PAM-D STAR 48.

4.4 STAR 48 (DM-2) Failure

On 17 December 1980, during the latter stages of its qualification programs (Q-8), the STAR 48 motor (DM-2) suffered a major failure shortly after propellant ignition. As of this date, an investigation is still underway; however, much

information is available upon which some preliminary conclusions have been drawn and this independent analysis based.

In essence, the first evidence of the impending failure was the observance of visible flame exiting perpendicular to the exit cone outer diameter downstream from nozzle closure 5.616 seconds after propellant ignition. Immediately thereafter the exit cone broke up and was destroyed. The submerged portion of the nozzle was expelled at approximately 18 seconds after propellant ignition with coincident termination of motor operation. Initial observations noted during the investigation are reflected in Figure 4.4.1. Based on those observations candidate failure causes consisted of pre-test or in-test damage, defective part(s), design deficiency and/or a combination of causes.

PRELIMINARY OBSERVATIONS

1. BALLISTIC PERFORMANCE NORMAL.
2. P AND P_c ARE CONSISTENT WITH LOSS OF EXIT CONE.
3. THROAT PACK PERFORMED OK.
4. NOZZLE INSULATOR ID ~~IS~~ AFFECTED BY FLOW.
5. EXIT CONE PHENOLIC INSULATOR FRAGMENTED; FRACTURE SURFACES SHOW LITTLE OR NO FLOW.
6. FLOW THROUGH SIDE OF EXIT CONE PERPENDICULAR TO NOZZLE AXIS OBSERVED NEAR CASE/CLOSURE INTERFACE.
7. NEAR INSTANTANEOUS FRAGMENTATION OF EXIT CONE AFTER FLOW OBSERVED THROUGH SIDE.
8. FRAGMENTS FROM FORWARD PORTION OF EXIT CONE HAVE NOT BEEN RECOVERED.
9. VISUAL EXAMINATION (INCLUDING ALCOHOL WIPE OF EXIT CONE FLOW SURFACE) OF MOTOR BEFORE FIRING REVEALED NO PROBLEMS.
10. NO EVIDENCE OF EXTERNAL EFFECT (SUCH AS CELL PRESSURE PERTURBATION) DURING FIRING.
11. NO EVIDENCE OF PROBLEMS IN TC PROCESSES DURING DM-2 MOTOR MANUFACTURE.
12. X-RAYS OF BILLET (FROM WHICH DM-2 EXIT CONE PRODUCED) CONTAIN INDICATIONS OF LOW DENSITY AREAS.
13. DM-2 NOZZLE TAG END SPECIMENS AND THOSE FROM GROUP EXHIBIT LOWEST RECORDED SBS AND COMPRESSIVE STRENGTH.
14. RECENT CONES FROM SUBSEQUENT LOTS HAVE LOW, OUT-OF-SPEC CIRCUMFERENTIAL TENSION VALUES.
15. TWO LOTS OF MATERIAL USED IN DM-2 CONE.

Figure 4.4.1

STAR 48 (DM-2) Failure Investigation Preliminary Conclusions and Analysis

The preliminary conclusions, based on the information amassed by the investigative body, are contained in Figure 4.4.1.1.

PRELIMINARY CONCLUSIONS

- o NO EVIDENCE OF DESIGN DEFICIENCY CONTRIBUTING TO FAILURE (ADDITIONAL THERMOSTRUCTURAL ANALYSES TO BE CONDUCTED)
- o NO EVIDENCE OF INCORRECT FABRICATION OR DAMAGE TO ANY PART(S) DURING NOZZLE ASSEMBLY OPERATIONS AT THICKOL
- o REVIEW OF RADIOGRAPHS INDICATES ALL NOZZLE ASSEMBLY COMPONENTS PROPERLY INSTALLED (GAPS CORRECT, RELATIVE POSITION OF PARTS CORRECT).
- o NO EVIDENCE OF PRETEST DAMAGE TO NOZZLE ASSEMBLY (RECENT STAR 37XF EXPERIENCE AT AEDC INDICATES SUCH PRETEST DAMAGE CAN OCCUR: ABILITY TO DETECT DAMAGE DEPENDS ON EXTENT AND NATURE OF DAMAGE).
- o NO EVIDENCE OF IMPROPER EXTERNAL ENVIRONMENT DURING DM-2 FIRING (CELL PRESSURE PERTURBATIONS, ETC.).
- o AVAILABLE DATA AND RADIOGRAPHS PERTAINING TO DM-2 EXIT CONE REVEAL SEVERAL AREAS OF CONCERN (LAMINATIONS MORE PRONOUNCED ON RADIOGRAPHS, SBS VALUES LOWER THAN PREVIOUS).
- o REVIEW AT HITCO INDICATES EXIT CONE MANUFACTURING PROCESS NOT WELL CONTROLLED (IMPERFECTIONS IN PATTERNS, CUT IN WRONG DIRECTION, ETC.).
- o EXIT CONE WITH UNDETECTED FLAWS MOST PROBABLE CAUSE OF FAILURE BASED ON EVIDENCE AVAILABLE AT THIS TIME.
- o RADIOGRAPHIC INSPECTION OF CARBON/CARBON EXIT CONE IS THE BEST NDT TECHNIQUE DEFINED TO DATE.

Figure 4.4.1.1

During our analysis of that information, three items were of special interest and significance.

- o The first appeared within the description of the various nondestructive testing methods and concerned reverberation. As stated, "successfully fired exit cone pieces reverberate when struck - DM-2 did not". This procedure is obviously quite easy to perform by both the vendor of the item at the

time of manufacture as well as the prime contractor during acceptance, and provides an ample indication that a manufacturing deficiency may exist. It would appear that little credence was placed on the results of that test as it pertained to DM-2.

- o The second appeared within the description of the radiograph test whereby all parts of the exit cone are checked for unusual indications. In this instance the comments stated, "the item(s) were free of unusual indications and the low density lines in the forward E.O.P. observed in S/N 011 (DM-2), although more pronounced, are characteristic of most cones." In our opinion, the words, "although more pronounced" are especially significant and again strongly suggest that an unusual indication may indeed have existed. In both of these cases, proper administration of quality control procedures appear to have been set aside and may have contributed to the failure of the DM-2 STAR 48 motor.

- o The third item concerned the potential of an outside facility force providing the impetus for motor failure. The test cell pressure contour was analyzed to determine whether or not an excessive back pressure may have initiated the chain of events which culminated in the failure. The test cell pressure contour confirmed that the test cell pressure was approximately .2 PSI from the time of motor ignition until the initiation of exit cone breakup (some five seconds later). At that point, the pressure jumped rapidly to approximately 1.5 PSI which coincided with our computed value of the cone exit plane pressure. The test cell is evacuated by a steam ejection system which in normal operation under test is assisted by the motor exhaust. The motor should be axially located within the test cell ejector system in a manner which permits the exit cone plane to geometrically match the steam ejector/mixing chamber. When

the cone separated, those geometric and flow patterns were upset leading to the rapid buildup of pressure (to 1.5 PSI) within the test cell. As such it was extremely unlikely that a facility pressure malfunction preceded the motor failure. Our analysis confirmed the investigative body's preliminary conclusion that "there was no evidence of an external effect (such as cell pressure perturbation) during firing".

In Figure 4.4.1.2, the cross-section of the nozzle of the STAR 48 DM-2 motor has been subdivided into a series of area ratio lines. In addition calculated pressures and Mach numbers which exist at those area ratio lines are also presented as well as a pressure distribution contour.

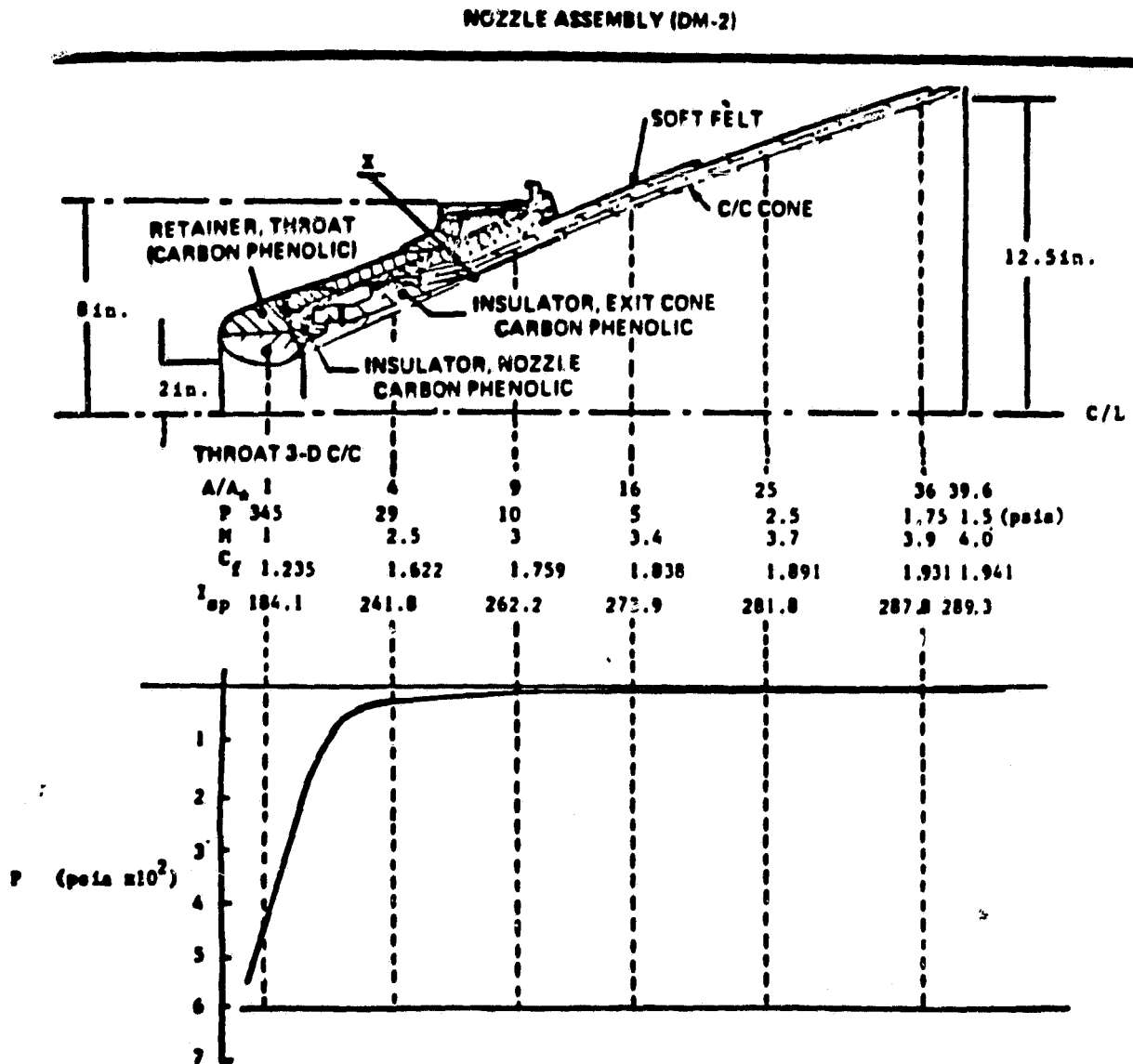


Figure 4.4.1.2

These values were computed using an average gamma value of $\gamma = 1.15$. Also of interest in Figure 4.4.1.2, is that point X marks the juncture of the carbon-carbon cone and the throat assembly. Apparently, the carbon-carbon layer is at its minimum thickness at point X; hence, is a critical design feature of the cone. With only a minor variation in the manufacturing process, the thickness at that point could be reduced below the acceptable limit thereby making that point extremely sensitive to pressure induced forces coupled with temperature induced stresses. These latter stresses could approach maximum values at approximately five (5) to ten (10) seconds after motor ignition.

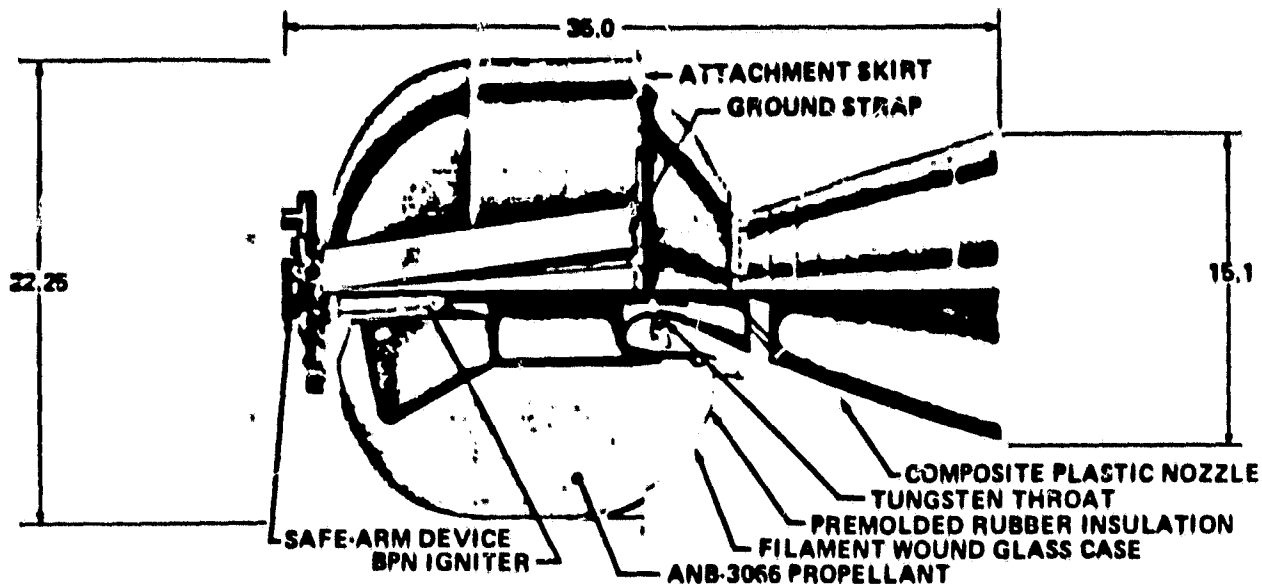
Based on our analysis of the available information, we conclude that the failure of the STAR 48 (DM-2) motor was prompted by procedural deficiencies during the manufacturing and/or testing processes which adversely impacted quality control. Moreover, a design weakness probably exists at the juncture point of the carbon-carbon cone and throat assembly. It is noted that additional thermo-structural analyses have been or are to be conducted which may serve to better define the extent of that design weakness.

5.0 SVM Motor Description

The SVM motor series SVM-1, -2, -4A, -5, -6, and -7 was developed by the Aerojet Solid Propulsion Company, a division of Aerojet General. Each of these motors is characterized by a glass filament (S-901) wound case, a composite propellant, front end ignition, and a high mass fraction. Figures 5.1 and 5.2 as supplied by Aerojet contain additional information regarding the SVM-2 motor description and performance characteristics.

The development of this series of high performance motors was based on nearly a decade of experience on the Minuteman program wherein that motor design was sized, optimized, and adapted for use as a high performance spacecraft motor possessing a specific impulse of 280-290 seconds. Overall this motor series is noted for its high reliability.

The SVM-2 motor was employed by NASDA as the AKM for the KIKU II, AYAME I, and AYAME II space flights. Although the latter two of these flights were deemed unsuccessful, there is no hard evidence which can point to AKM failure as the governing causal event.



INTRODUCTION

This Space Vehicle Motor (SVM-2) was developed and qualified for placing the Intelsat III communications satellite in a precise geosynchronous orbit. The SVM-2 is qualified for use as an apogee boost motor or other space use requiring a precision-made controlled-impulse motor. During the program, 28 motors were built, with 20 tested and 8 delivered for flight use. This program scope could be substantially reduced for verification testing of similar motors in this impulse range.

MOTOR DESCRIPTION

The SVM-2 is a 22.25-in.-dia motor delivering a total impulse of 86,900 lbf-sec with an average thrust of 3,140 lbf over a total duration of 27.6 sec. This performance is provided at +60°F and vacuum. The motor weighs 350.2 lbm and is 35.0 in. in overall length. Motor attachment to the spacecraft is accomplished by an integral, aluminum thrust ring that can be modified to suit specific spacecraft requirements. The light-weight motor case is wound from S-901 glass filament and incorporates integral forward and aft aluminum polar bosses for igniter and nozzle attachment. Motor length is easily varied by an increase or decrease of the case midsection length, thus providing a range of propellant loading for impulse flexibility. The submerged nozzle consists of an aluminum housing, supporting a reinforced-phenolic entrance section and exit cone, with a silver-infiltrated tungsten throat for precise control of the thrust vector during firing. The propellant/liner/insulation system is the same as used in the SVM-1, -4A and -5 motors and has a real time base experience in excess of 8 years gained on the Aerojet Minuteman programs. The propellant, a production carboxy-terminated polybutadiene (CTPB), has a demonstrated 3-sigma total impulse variability of

less than 0.75% in all SVM motors tested. The internal case insulation is premolded from a silica-filled polybutadiene material, which has been fully qualified and characterized in its erosive and thermal properties under actual motor conditions. The liner is a filled imine-cured CTPB binder. This system has been demonstrated in static and flight tests of many SVM and Minuteman motors. The igniter consists of a tape-wrapped glass-phenolic chamber containing boron potassium nitrate (BPN) as the pyrotechnics for both the initiator and main charges. Except for size, the igniter is the same as that used in SVM-4A and -5 motors. The safe-and-arm device, with two electrical initiators (1 amp/1 watt), is a fully qualified unit meeting all requirements for use at the Air Force Eastern Test Range (AFETR). It is also used in the SVM-4A and -5 motors. All materials (glass filament, aluminum, glass- and carbon-reinforced phenolics, tungsten throat, rubber insulation, propellant, BPN) have been proven in several hundred other Aerojet motors for strategic, tactical, and space applications.

TEST ENVIRONMENT

The SVM-2 motor has been thoroughly tested during qualification. Results of sinusoidal and random vibration in three axes and flights of eight motors demonstrated motor ruggedness for shipping, handling, and flight environments. Four and one half temperature cycles from +20 to +100°F qualify the motor for the temperature range to be expected in normal use. Twenty motors have been test fired at a simulated altitude of 100,000 ft while spinning and at temperatures of +20 to +100°F. All motors successfully performed to specification requirements. In addition, five Intelsat III communication satellites have been successfully placed into geosynchronous orbit.

Figure 5.1

PERFORMANCE (60° F VACUUM, NOMINAL)

| | |
|--|--------|
| Total Impulse, lbf-sec | 86,900 |
| Total Duration, sec | 27.6 |
| Average Thrust, lbf | 3140 |
| Maximum Thrust, lbf | 4830 |
| Average Pressure, psia | 296.5 |
| Maximum Pressure, psia | 456 |
| Propellant Delivered Specific Impulse, ⁽¹⁾ lbf-sec/lbm | 283.8 |
| Motor Delivered Specific Impulse, ⁽²⁾ lbf-sec/lbm | 280.8 |
| Ignition Time, sec | 0.06 |
| Qualified Spin Rate, rpm ⁽³⁾ | 110 |

TEST ENVIRONMENT

| | |
|---------------------------|-------------|
| Operating Temperature, °F | +20 to +100 |
| Storage Temperature, °F | +20 to +120 |
| Axial Acceleration, g | 14 |
| Lateral Acceleration, g | 2 |
| Vibration Qualified | Yes |

ROCKET CLASSIFICATION

(Motor with igniter and safe-arm device) **B**

WEIGHT

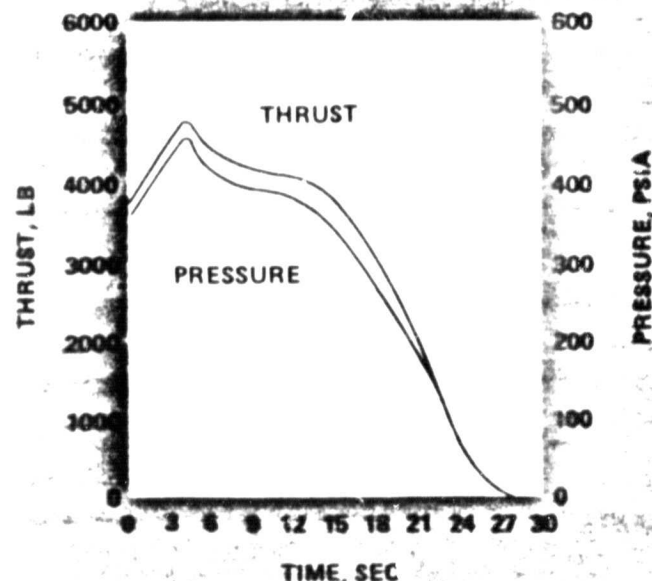
| | |
|--|-------|
| Loaded, lbm | 350.2 |
| Propellant, lbm | 305.6 |
| Burnout, lbm | 40.75 |
| Mass Fraction (Includes 4.65-lbm safe-arm device) | 0.873 |

CG DISTANCE FROM FORWARD BASE OF SKIRT

| | |
|--------------|------|
| Loaded, in. | 4.98 |
| Burnout, in. | 1.68 |

MBA - WCE AVG. OF 8 MOTORS

| | |
|------------------------------|------|
| Static, lb-in. | 1.4 |
| Dynamic, lb-in. ² | 11.1 |



THRUST AND PRESSURE VS TIME, 60° F, VACUUM

THRUST ALIGNMENT

| | |
|---------------------|---------|
| Angularity, in./in. | <0.0025 |
| Throat Offset, in. | <0.020 |

PROPELLANT

| | |
|-----------------------|------|
| Type | CTPB |
| Solids Content, % | 88 |
| Ammonium Perchlorate | 73 |
| Aluminum | 15 |
| Flame Temperature, °F | 5836 |

NOZZLE

| | |
|-------------------------------|-----------|
| Type | Contoured |
| Submergence, % | 23.5 |
| Throat Area, in. ² | 5.96 |
| Expansion Ratio | 28 |

CHARGE

| | |
|------------------------------------|-----|
| Main charge, BPN pellets, gm | 136 |
| Initiator charge, BPN granules, gm | 8 |

SAFE ARM DEVICE

Qualified to AFETRM 127-1

MOMENTS OF INERTIA, LOADED (LB-IN.²)

| | |
|--------------|--------|
| Roll | 21,110 |
| Pitch or Yaw | 21,024 |

RELIABILITY

| | |
|-----------------------|-------|
| Observed (25 firings) | 1.000 |
|-----------------------|-------|

(1) I_{sp} = $\frac{\text{Total area under thrust-time curve less impulse due to inert weight loss}}{\text{Total propellant burned}}$

(2) I_{sd} = $\frac{\text{Total area under thrust-time curve}}{\text{Total weight loss of motor}}$

(3) If desired, rpm can be increased.

- IMPULSE FLEXIBILITY
- SPACE-PROVEN PROPELLANT SYSTEM
- PRECISE THRUST VECTOR
- STRINGENT BALANCE AND IMPULSE CONTROL

PERFORMANCE (60° VACUUM NOMINAL)

| | |
|--|--------|
| Total Impulse, lbf-sec | 86,900 |
| Total Duration, sec | 27.6 |
| Average Thrust, lbf | 3140 |
| Maximum Thrust, lbf | 4830 |
| Average Pressure, psia | 296.5 |
| Maximum Pressure, psia | 456 |
| Propellant Delivered Specific Impulse (1) lbf-sec/lbm | 283.8 |
| Motor Delivered Specific Impulse (2) lbf-sec/lbm | 280.8 |
| Ignition Time, sec | 0.06 |
| Qualified Spin Rate, rpm (3) | 110 |

OPERATING ENVIRONMENT

| | |
|---------------------------|-------------|
| Operating Temperature, °F | +20 to +100 |
| Storage Temperature, °F | +20 to +120 |
| Axial Acceleration, g | 14 |
| Lateral Acceleration, g | 2 |
| Vibration Qualified | Yes |

TOP CLASSIFICATION

(Motor with igniter and safe-arm device) **B**

WEIGHT

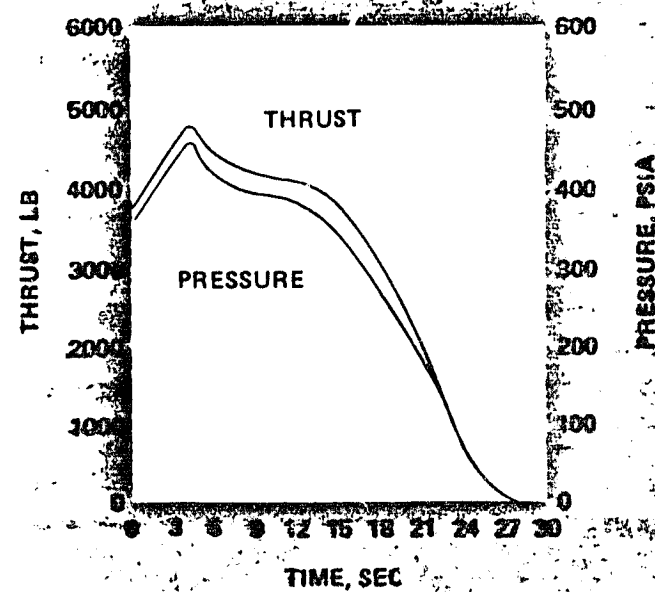
| | |
|-------------------------------------|-------|
| Loaded, lbm | 350.2 |
| Propellant, lbm | 305.6 |
| Burnout, lbm | 40.75 |
| Mass Fraction | 0.973 |
| (Includes 4.65-lbm safe-arm device) | |

CG DISTANCE FROM FORWARD BASE DESKIN

| | |
|--------------|------|
| Loaded, in. | 4.98 |
| Burnout, in. | 1.68 |

MOMENT OF INERTIA (AVG OF 2 MOTORS)

| | |
|------------------------------|------|
| Static, lb-in. | 1.4 |
| Dynamic, lb-in. ² | 11.1 |



THRUST ALIGNMENT

| | |
|---------------------|---------|
| Angularity, in./in. | <0.0025 |
| Throat Offset, in. | <0.020 |

PROPELLANT

| | |
|-----------------------|------|
| Type | CTPB |
| Solids Content, % | 88 |
| Ammonium Perchlorate | 73 |
| Aluminum | 15 |
| Flame Temperature, °F | 5836 |

TYPE

| | |
|-------------------------------|-----------|
| Type | Contoured |
| Submergence, % | 23.5 |
| Throat Area, in. ² | 5.96 |
| Expansion Ratio | 28 |

CHARGE

| | |
|------------------------------------|-----|
| Main charge, BPN pellets, gm | 136 |
| Initiator charge, BPN granules, gm | 8 |

SAFE ARM DEVICE

Qualified to AFETRM 127-1

MOMENTS OF INERTIA (LOADED, LBM)

| | |
|--------------|--------|
| Roll | 21,110 |
| Pitch or Yaw | 21,024 |

RELIABILITY

Observed (25 firings) **1.000**

(1) I_{sp} = $\frac{\text{Total area under thrust-time curve less impulse due to inert weight loss}}{\text{Total propellant burned}}$

(2) I_{sd} = $\frac{\text{Total area under thrust-time curve}}{\text{Total weight loss of motor}}$

(3) If desired, rpm can be increased.

- IMPULSE FLEXIBILITY
- SPACE-PROVEN PROPELLANT SYSTEM
- PRECISE THRUST VECTOR
- STRINGENT BALANCE AND IMPULSE CONTROL

The Universal Systems, Inc. study entitled "Implications of Ayame Failure for the Delta Project", dated September 7, 1979, contains detailed information relative to the failure of the Ayame I on/about February 9, 1979 during the firing of the AKM. In analyzing the Ayame I failure, the flight profile of the successful KIKU II engineering test satellite (launched on February 23, 1977) was used as a baseline since the KIKU II configuration was essentially the same as the Ayame I. Based on that analysis it was concluded that the YO-weight deployed prematurely during the spin-up of the third stage/spacecraft. Upon separation of the spacecraft from the third stage, a collision between the two bodies took place when "chuffing" of the third stage motor occurred. Although the spacecraft did not suffer catastrophic damage, "coning" was experienced and the rotational speed was reduced from 90 to 60 rpm. Communications from the spacecraft continued to function until shortly after the firing of the AKM, some two days after the collision. Lastly, it should be noted that the spacecraft was later found to be in near GEO orbit.

Ayame II failed in almost the identical manner with the exception that the third stage/spacecraft separation was without incident. To date, the Ayame II spacecraft has not been located although we suspect that it is also in near GEO orbit.

Figure 6.1 contains a listing of the most probable causes for the mission failures of the Ayame I and Ayame II, as well as the destruction of the STAR 48 (DM-2) motor during test. Our comments and conclusions based on our analysis of available data are also included. We are convinced that from a technical and engineering point of view there is no correlation between the Ayame failure modes and the STAR 48 (DM-2). However, the close similarity between the two failures (loss of signal) of Ayame I and II and our analysis of the associated data lead us to believe the spacecraft AKM functioned properly in both cases, and the failures can probably be attributed to some malfunction within the electrical system.

As an aside, it is further noted that the RCA Satcom III C (Delta 150) apparently failed in an identical manner in December 1979. That failure is to become the subject of a follow-on report.

POTENTIAL FAILURE MODES AYAME I, AYAME II, STAR-48 (DH-2)

| TYPE FAILURE | CAUSATIVE FACTOR(S) | PROBABLE EFFECT IF OCCURRING | ANALYSIS | CONCLUSION |
|---|---|--|--|--|
| A. Propellant Grain/Case Bond Crack or Separation | <ol style="list-style-type: none"> 1. Improper Fabrication and Curing. 2. Faulty Ingredients. 3. Improper Handling. | <p>Increased rate of burning with attendant higher chamber pressure</p> | <ol style="list-style-type: none"> 1. Carried to an extreme, could cause rupture with complete motor failure 2. Composite propellant could be extinguished 3. No evidence of this type of event causing mission failure within AYAME I, AYAME II, or STAR 48 (DH-2). (KIKU II was a success) | <p>Extremely unlikely to have occurred.</p> |
| B. Igniter Assembly/ Ignition Transients | <ol style="list-style-type: none"> 1. Improper igniter formulation 2. Interruption of explosive train | <ol style="list-style-type: none"> 1. Propellant fails to ignite. 2. Ignition transients are always present, but in this case, the transients would develop a chamber pressure in excess of that which the motor case could withstand. | <ol style="list-style-type: none"> 1. No evidence of AKM failure to ignite in AYAME I or AYAME II (KIKU II was a success) 2. No evidence of ignition transients exceeding specified limits in AYAME I, AYAME II or STAR 48 (DH-2) 3. KIKU II, AYAME I and AYAME II AKMs all functioned properly based on telemetry/test data reflecting nominal chamber pressure traces. | <p>Extremely unlikely to have occurred.</p> |
| C. Cone Rupture | <ol style="list-style-type: none"> 1. Improper fabrication 2. Design weakness 3. Improper handling 4. Improper materials 5. Faulty quality control inspection techniques | <ol style="list-style-type: none"> 1. Reduction in thrust 2. Prandtl-Meyer expansion damage | <ol style="list-style-type: none"> 1. No evidence of cone failure/damage in AYAME II 2. Possible damage in AYAME I 3. KIKU II successful 4. Loss of cone - STAR 48 (DH-2) 5. For AYAME I, no evidence of adverse impact on performance of AKM. 6. Faulty quality control inspection techniques for STAR 48 (DH-2) See paragraph 4.4 this report. 7. Possible STAR 48 (DH-2) design weakness. See paragraph 4.4 this report. | <ol style="list-style-type: none"> 1. Unlikely that cone failure can be attributed to AYAME I or II mission failures 2. Quality control inspection techniques applicable to STAR 48 need to be rectified 3. STAR 48 cone design integrity needs to be confirmed. |
| D. Electric Power System | <ol style="list-style-type: none"> 1. Improper grounding (ground loops) 2. Excessive environmental factors during flight profile (vibration, thermal stress, etc.) 3. Improper countdown procedures/test 4. Excessive electrical surge or drain | <p>Communication failure</p> | <p>A potential existed for the formation of a low voltage plasma in vacuum conditions. If so, continual arcing could prematurely drain the available power supply thereby causing low voltage to be delivered to the communications equipment. Since the "C" band beacon is more sensitive to low voltage than the telemetry equipment, the "C" band beacon would cease to function prior to the telemetry system. Normally such arcing would not occur unless provoked by some stimulus. Carbon fibers released during the ablative process might possibly provide that stimulus.</p> | <ol style="list-style-type: none"> 1. Electrical power failure is the most probable cause of AYAME I and AYAME II mission failures. 2. A test program to ascertain the impact of carbon fibers released through the ablative process or by cone rupture on electrical power systems in vacuum conditions is desirable. |

Figure 6.1

7.0

Massive Nozzle Failure Postulation

Rather than attempting to examine various apogee kick motors, i.e., SVM-2, SVM-7, STAR 30B, etc., and postulate specific massive nozzle failures for each, we have elected to base our postulation on a progression of failures of the nozzle exit cone and the resultant changes to the area ratio between the nozzle exit cone and the nozzle throat. Accordingly, Figure 7.1 is a table which reflects the loss of thrust coefficient as more of the nozzle is progressively lost. It is to be noted that the first two entries are descriptive of the STAR 48 PAM configurations. All of the values were derived using a gamma value of 1.15 and a chamber pressure of 600 psia under vacuum conditions. The 600 psia chamber pressure is a nominal value for high performance motors to include the SVM-2, SVM-7, STAR 48, and STAR 30B.

| A/A* | Pe/Pc | C _F | NOTES |
|--------------------|--------|----------------|--|
| PAM-D 8" EXTENSION | | | |
| 51.84 | .00167 | 1.968 | A/A* = $\frac{\text{Nozzle station area}}{\text{throat area}}$ |
| PAM-A SHORT NOZZLE | | | |
| 39.6 | .0025 | 1.941 | Pe/Pc = $\frac{\text{Station exit pressure}}{\text{Chamber pressure}}$ |
| 36 | .0029 | 1.931 | |
| 25 | .0042 | 1.891 | C _F = Thrust coefficient |
| 16 | .0083 | 1.838 | |
| 9 | .01667 | 1.759 | |
| 4 | .04833 | 1.622 | |
| 1 | .575 | 1.235 | |

Figure 7.1

In Figure 7.2, the effect on the transfer orbit of the changes to a number of the area ratio and thrust coefficients from Figure 7.1 are identified. The symbology used within Figure 7.2 is defined below.

- A/A* = area ratio
 C_F = Thrust coefficient
 R_a = Radius of apogee from center of earth in statute miles
 R_p = Radius of perigee from center of earth in statute miles
 V_a = velocity at apogee in feet/second
 V_p = velocity at perigee in feet/second
 e = eccentricity of orbit calculated by the equation $e = \frac{1-R_p/R_a}{1+R_p/R_a}$
 Period = time elapsed for one orbit

In developing the data a 100 nautical mile (114 statute miles) circular LEO was used as the standard for evaluation of the third stage loss of performance. Likewise the change in velocity (V) required to move from LEO to a transfer orbit possessing the correct apogee distance of 26,275 statute miles was 8087 feet/second.

Transfer Orbit Performance Loss

| A/A* | C _F | R _a /V _a | R _p /V _p | e | Period |
|-------------------|----------------|--------------------------------|--------------------------------|----------|------------------------------------|
| STD no loss 52 | 1.968 | 26,275/ 5231.2 | 4,079/ 33,679 | 0.731238 | 10.5342 hrs 10 hrs 32 min 3 sec |
| 25 | 1.891 | 23,010/ 5,917 | 40,790/ 33,380 | 0.698845 | 8.8816 hrs 8 hrs 52 min 54 sec |
| 9 | 1.759 | 18,845/ 7,108 | 4,079/ 32,838 | 0.665565 | 6.7457 hrs 6 hrs 44 min 44 sec |
| 4 | 1.622 | 15,733/ 8,368 | 4,079/ 32,375 | 0.588229 | 5.5547 hrs 5 hrs 33 min 17 sec |
| 1 | 1.235 | 10,375/ 12,064 | 4,079/ 30,685 | 0.435589 | 3.4615 hrs 3 hrs 27 min 41 sec |

Figure 7.2

If solid motors are used for the third stage and AKM and the third stage/ spacecraft are spin stabilized, the impact of the degradation of performance as shown in Figures 7.2 and 7.3 would probably lead to mission failure.

In Figure 7.3 the effect of the changes to the area ratio and coefficients from Figure 7.1 on the orbit parameters are identified. The symbology used within Figure 7.3 is the same as for Figure 7.2. In developing the data reflected in Figure 7.3, a change in velocity of 4,860 feet per second was used as the standard to move from an ideal equatorial transfer orbit to GEO.

AKM Performance Loss

| A/A* | C _F | R _a /V _a | R _p /V _p | e | Period |
|-------------------|----------------|--------------------------------|--------------------------------|----------|--|
| STD no loss 52 | 1.968 | 26,275/ 10,091 | 26,275/ 10,091 | 0 | 24 hrs 00 min 00 sec |
| 25 | 1.891 | 26,275/ 9,858 | 23,985/ 10,799 | 0.045563 | 22,447 hrs 22 hrs 26 min 41 sec |
| 9 | 1.759 | 26,275/ 9,575 | 21,516/ 11,693 | 0.099576 | 20.8113 hrs 20 hrs 48 min 41 sec ² |
| 4 | 1.622 | 26,275/ 9,237 | 19,948/ 12,809 | 0.162025 | 19.1567 hrs 19 hrs 9 min 24 sec ² |
| 1 | 1.235 | 26,275/ 8,281 | 13,340/ 16,310 | 0.326504 | 15.7060 hrs 15 hrs 42 min 22 sec ² |

Figure 7.3

In this attempt to establish a correlation between the Ayame I, Ayame II and STAR 48 (DM-2) failures, the ratio between the areas of the nozzle exit plane and the nozzle throat was used as the common analytical vehicle and the successful KIKU II mission flight profile serving as the baseline for comparison. Early in the analytical process, it became evident the STAR 48 failure bore no relation to the Ayame I and II failures. Nevertheless the STAR 48 test data did provide values which permitted the pertinent use of descriptive elliptical equations and properties as well as earth orbital dynamic equations and properties (See Appendix 3 and 4). From these equations, the impacts on both transfer and GEO orbital parameters due to progressive losses of the nozzle cone (as they affected the area ratio) were computed.

Applying the computations to Ayame I, it first appeared that the perigee of the GEO orbit reported by NORAD (subsequent to loss of signal) might have been caused by the loss of approximately one-third of the nozzle (a reduction of 50% in the area ratio). Such a loss was plausible depending on the force of collision between the third stage and the spacecraft prior to AKM firing. However, the increase in the GEO apogee, as compared to the apogee of the transfer orbit, could not have occurred if a partial loss of AKM nozzle had in fact been experienced. Ultimately we concluded a more logical explanation to account for the changes in the GEO apogee and perigee was the orientation of the spacecraft due to the coning caused by the collision. Assuming an approximate 5° pitch orientation toward earth at time of AKM firing, a GEO orbit with the Ayame I parameters reported by NORAD was entirely feasible. We feel this explanation to be more representative of what happened to the Ayame I spacecraft. We attributed the loss of signal to an unexplained electrical power failure.

With respect to Ayame II, there is still little data available upon which to reliably establish a failure mode. Communication with the spacecraft ceased during the mid-eight second burn of the AKM but no hard evidence exists of either motor malfunction or spacecraft "coning" prior to the AKM firing. To date the

spacecraft remains unlocated. Since the spacecraft was in a nominal transfer orbit at time of AKM firing, we are of the opinion the spacecraft is probably in a GEO orbit which deviates to some degree from the planned parameters. We believe an unexplained electrical power failure also caused the termination of signal from the Ayame II spacecraft.

From our analysis, we recommend:

(1) Quality control measures and all procedural activities he reviewed with the objective of "tightening" existing techniques. The focus of this effort to be placed on the system contractor.

(2) More emphasis be placed on government monitoring of contractor/subcontractor activities.

(3) Improve communication between government agencies relative to programmed operations for the purpose of increasing interdepartmental awareness and potential support.

(4) The application of acoustic holography testing be evaluated for potential application to nozzle acceptance procedures.

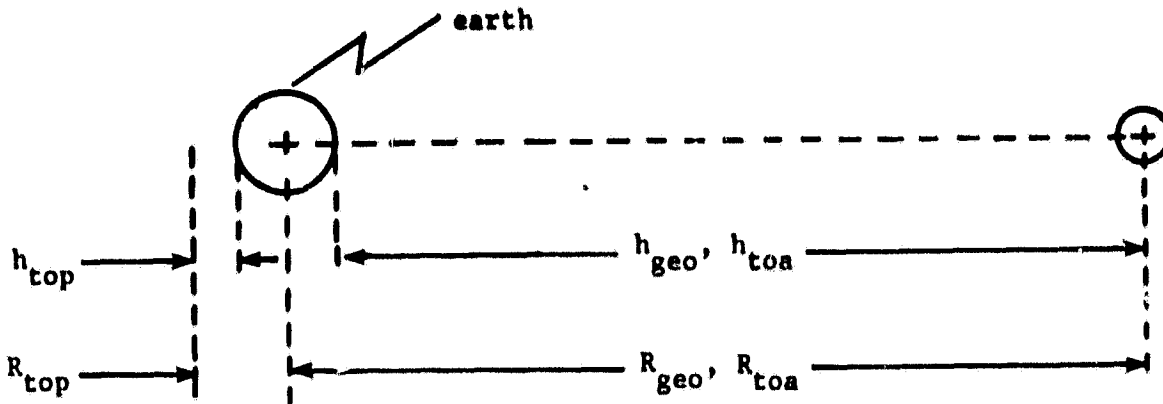
APPENDIX I

EQUATION SYMBOLOGY WITHIN APPENDICES

| | | |
|--------------|---|---|
| e_{geo} | - | Eccentricity of geocentric earth orbit |
| e_{to} | - | Eccentricity of transfer orbit |
| h_{geo} | - | height of geocentric earth orbit |
| h_{toa} | - | height of transfer orbit apogee |
| h_{top} | - | height of transfer orbit perigee |
| R_a | - | radius of apogee when angle of radius vector equals 0° |
| R_{earth} | " | radius of earth |
| R_{geo} | - | radius of geocentric earth orbit |
| R_p | - | radius of perigee when angle of radius vector equals 180° |
| R_{toa} | - | radius of transfer orbit apogee |
| R_{top} | - | radius of transfer orbit perigee |
| V_a | - | velocity at apogee in feet/second |
| V_{esc} | - | velocity for escape in feet/second |
| V_{geo} | - | velocity at geocentric earth orbit in feet/second |
| V_h | - | velocity along the radius vector at a specific orbit point |
| V_θ | - | velocity perpendicular to the radius vector at the same specific orbit point corresponding to V_h |
| V_p | - | velocity at perigee in feet/second |
| $V_{e surf}$ | - | velocity at surface of earth at equator in feet/second |
| V_{toa} | - | velocity at transfer orbit apogee in feet/second |
| V_{top} | - | velocity at transfer orbit perigee in feet/second |
| ω | - | angular rate in seconds |

APPENDIX II

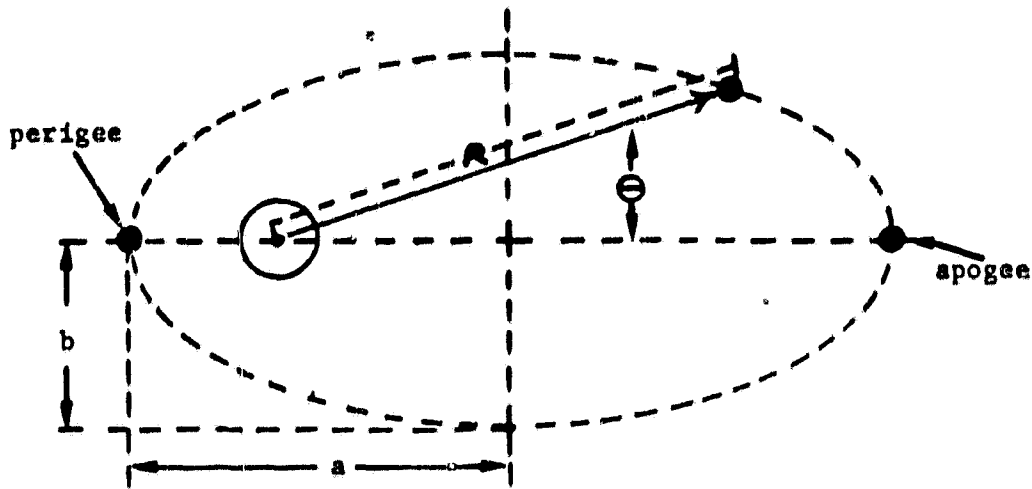
TRANSFER AND GEOCENTRIC EARTH ORBIT VALUES



| | | |
|--------------------|---|-----------------------------------|
| h_{geo}, h_{toa} | = | 35,786 km or 22,236 statute miles |
| R_{geo}, R_{toa} | = | 42,284 km or 26,275 statute miles |
| h_{top} | = | 185.3 km or 115.2 statute miles |
| R_{top} | = | 6566 km or 4080 statute miles |
| ω_{geo} | = | 0.000072722 radians/sec. |
| $V_{e\ surf}$ | = | 1522 ft./sec. @ equator |
| V_{geo} | = | 10,086 ft./sec. |
| e_{geo} | = | 0 |
| e_{to} | = | 0.73118 |
| V_{top} | = | 33,602 ft./sec. |
| V_{toa} | = | 5217.8 ft./sec. |
| R_{earth} | = | 3965 statute miles |

APPENDIX III

DESCRIPTIVE ELLIPTIC EQUATIONS & PROPERTIES



Defining Equations

$$p \equiv \frac{b^2}{a}$$

$$e \equiv \sqrt{1 - \frac{b^2}{a^2}}$$

Basic Polar Coordinate Equation

$$R = \frac{\frac{b^2}{a}}{1 - \cos\theta \sqrt{1 - \frac{b^2}{a^2}}} = \frac{p}{1 - e \cos\theta}$$

Derived Related Descriptive Equations

$$\left. \begin{aligned} R_p &= \frac{p}{1+e} \\ R_a &= \frac{p}{1-e} \end{aligned} \right\} \rightarrow \frac{R_p}{R_a} = \frac{1-e}{1+e} \text{ or } e = \frac{1 - \frac{R_p}{R_a}}{1 + \frac{R_p}{R_a}}$$

or solving for p:

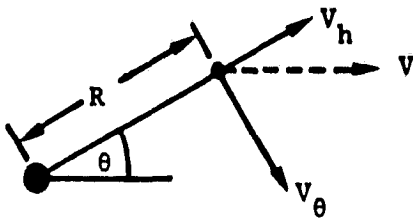
$$p = R_p (1 + e) = R_a (1 - e)$$

Note: Cosine $\theta = 1$ when $\theta = 0^\circ$ and 180°

APPENDIX IV

EARTH ORBITAL DYNAMIC EQUATIONS & PROPERTIES

The basic conservation of energy equation used for analysis in this report for orbit injection is:



| | |
|--|---|
| <p>in orbit conditions</p> $\underbrace{\frac{1}{2} (v_h^2 + v_\theta^2)}_{\text{kinetic energy}} + \underbrace{\left(gR_e \left(1 - \frac{R_e}{R} \right) \right)}_{\text{potential energy}}$ | <p>injection conditions (i)</p> $= \underbrace{\frac{v_1^2}{2}}_{\text{kinetic energy}} + \underbrace{gR_e \left(1 - \frac{R_e}{R_1} \right)}_{\text{potential energy}}$ |
|--|---|

Noting that the earth escape velocity can be expressed as:

$$v_{esc}^2 = 2gR_e$$

the energy may be written in the following forms:

$$\frac{v^2}{v_{esc}^2} = \frac{v_h^2 + v_\theta^2}{v_{esc}^2} = \frac{v_1^2}{v_{esc}^2} + \left(\frac{R_e}{R} - \frac{R_e}{R_1} \right)$$

Further noting that $V_h = 0$ at apogee and at perigee where $V_1 = V_p$ and $R_1 = R_p$ the energy equation takes the form of:

$$\frac{v_a^2}{v_{esc}^2} = \frac{v_p^2}{v_{esc}^2} + \left(\frac{R_e}{R_a} - \frac{R_e}{R_p} \right)$$

Taking into account that the moment of momentum at perigee must equal that at apogee, i.e.:

$$R_p V_p = R_a V_a$$

it follows that:

$$\frac{v_p^2}{v_{esc}^2} = \frac{\frac{R_e}{R_p}}{1 + \frac{R_p}{R_a}} \quad \text{OR} \quad \frac{v_a^2}{v_{esc}^2} = \frac{R_p^2}{R_a^2} \left(\frac{\frac{R_e}{R_p}}{1 + \frac{R_p}{R_a}} \right)$$

or noting that:

$$\frac{R_p}{R_a} = \frac{V_a}{V_p} = \frac{1-e}{1+e}$$

the latter two equations may be reduced to:

$$\frac{V_p^2}{V_{esc}^2} = \frac{\frac{R_e}{R_p}}{1 + \frac{V_a}{V_p}} = \frac{\frac{R_e}{R_p}}{1 + \frac{1-e}{1+e}}$$

or solving for V_a/V_p :

$$\frac{V_a}{V_p} = \frac{\frac{R_e}{R_p}}{\frac{V_p^2}{V_{esc}^2}} = 1$$